Available online at www.sciencedirect.com

ScienceDirect

IFAC PapersOnLine CONFERENCE PAPER ARCHIVE

IFAC PapersOnLine 56-3 (2023) 229–234

Vibration reduction of semisubmersible floating wind turbine using optimized tuned mass and tuned inerter dampers

Duncan L. Lambert * **Lei Zuo** **

* *Virginia Polytechnic Institute and State University, Blacksburg, VA 24061 USA (e-mail: Duncan22@vt.edu).*

** *University of Michigan, Ann Arbor, MI 48109 USA (e-mail: leizuo@umich.edu)*

Abstract: Over the past decade, offshore wind has positioned itself as one of the most promising renewable energy markets. While this field is currently dominated by fixed-bottom wind turbines located within a limited depth range, floating turbines are showing promise as a way to capture the more developed wind profiles available in deeper waters. Currently, the main challenge with floating offshore wind is that the systems experience larger ultimate loads compared to fixed bottom turbines. These larger loads are caused by the increased motion inherent with floating structures. This study looks to analyze the effects that traditional and inerter based structural control methods can have on reducing the motion of floating offshore wind turbines. Models are developed adding tuned mass dampers (TMD) and tuned inerter dampers (TID) into the three main columns of the semisubmersible platform. Results showed that for free decay tests, heave and pitch RMS values were reduced significantly by the addition of passive structural control. The inerter based structural control consistently outperformed traditional TMD and allowed for similar performance with significantly reduced physical mass values.

Copyright © 2023 The Authors. This is an open access article under the CC BY-NC-ND license (https://creativecommons.org/licenses/by-nc-nd/4.0/)

Keywords: Offshore wind, Structural control, Tuned mass damper, Tuned inerter damper, Free decay, Optimization

1. INTRODUCTION

Many of the world's most pressing challenges today revolve around a need for clean energy. Whether the challenge is as straightforward as providing affordable energy to developing countries, or as complex as attempting to stabilize global warming, the focal point is still, a need for clean energy. The world's focus on tackling these challenges has intensified since the turn of the century, as evidenced by global agreements such as the Kyoto Protocol and the Paris Agreement. This focus has resulted in an exponential increase in funding, research, and growth in several different renewable energy fields.

Offshore wind refers to the application of land-based platforms in offshore regions through the use of fixed bottom foundations or floating platforms. As a whole, the offshore wind market has boomed in recent years, growing to a total installed capacity of over 50,000 MW over the last two decades (Musial et al. (2022)). While this market is currently dominated by fixed-bottom wind turbines placed close to the shore, data shows that the use of floating platforms is expected to increase significantly over the next 5 years (Musial et al. (2022)). This increase is due to the fact that wind speeds are much higher further offshore, in deeper water that is not suitable for fixed bottom designs (Zhou et al. (2023)). Also, the availability of sites for wind farms is greater further offshore. There are currently several floating platform designs used, though one in particular seems poised to dominate this market and that is the semisubmersible platform design. The semisubmersible platform is a concept originally developed by the University of Maine and is projected to support the vast majority of floating offshore wind farms by 2028 (Robertson et al. (2014)). While this platform design currently outperforms other concepts, it still experiences many of the same shortcomings that characterize offshore floating wind turbines. The most severe shortcoming being that the semisubmersible platform experiences larger ultimate loads for many critical bending moments compared to land based or fixed bottom turbines (Robertson and Jonkman (2011)). This increased loading comes from the fact that the semisubmersible platform is a moored structure and therefore can experience more motion than a fixed structure. In other words, more motion in critical degrees of freedom such as pitch and heave, means higher loads, which means a shorter lifespan. Although these larger motions could be remedied through the implementation of structural control, a concept that has been used to reduce motion in structures for over 100 years.

Structural control has largely been used to mitigate wind and earthquake induced motion in large buildings through the addition of motion reducing subsystems. The most famous of these subsystems is the passive tuned mass damper (TMD), that when tuned effectively can cancel out the majority of motion experienced by a building (Frahm (1911)). Examples of buildings that utilize TMDs for motion reduction includes Taipei 101 in Taiwan and Park Tower in Chicago. In recent years, the inerter, a

2405-8963 Copyright © 2023 The Authors. This is an open access article under the CC BY-NC-ND license.
Peer review under responsibility of International Federation of Automatic Control.
10.1016/j.ifacol.2023.12.029

device that generates a force proportional to a relative acceleration, has begun to be integrated into structural control subsystems (Smith (2002)). The addition of the inerter has shown both an increase in performance and a reduction in the physical mass needed for structural control subsystems. Several acronyms exist for different inerter based structural control methods, for this study they will be referred to as tuned inerter dampers (TID). Research into incorporating structural control into offshore floating wind platforms does exist, though is largely focused on adding a single fore-aft TMD into the nacelle or platform (Stewart (2012), Lackner and Rotea (2011), Si et al. (2014)). Moreover, research into applying inerter based structural control into offshore floating wind platforms is even more limited (Hu et al. (2018), Ma et al. (2020)). And at this time no study exists analyzing the effects of adding three traditional or inerter based structural control subsystems into the three primary columns of the semisubmersible platform design.

This study looks to provide an in depth analysis studying the effects of implementing a traditional passive TMD system into the three columns of the OC4 semisubmersible platform design. The traditional TMD system is compared to an optimal TID configuration. The TMDs and TIDs are oriented within the three columns such that they move vertically in the z-direction. Three different models are derived and validated. These models are then used to conduct an optimization for a heave and pitch free decay test. The results of these free decay optimizations are compared between control configurations in order to determine their effectiveness at reducing the platforms turbines motion.

The contents of this paper are organized as follows. Section 2 provides an introduction to the hydrodynamics formulation. Section 2 also includes the derivation and validation of all TMD and inerter based wind turbine models. Section 3 presents and discusses the results of two free decay test optimizations. Lastly, section 4 states the key conclusions.

2. MODEL DERIVATIONS

2.1 Hydrodynamics Formulation

For this study, all wave related forces are calculated using linear hydrodynamic coefficients obtained from ANSYS AQWA. AQWA is a frequency-domain potential flow Boundary Element Method (BEM) solver, where BEM solutions are determined by solving the Laplace equation for the velocity potential. The primary assumptions of this method are that the flow is inviscid, incompressible, and irrotational. A more detailed look into the theory behind BEM solvers can be found in the WAMIT user manual Lee and Newman (2013).

The hydrodynamic forces used in this study include $F_{rad}(t)$, the force and torque resulting from wave radiation, $F_B(t)$, the buoyancy force and torque, and $F_{exc}(t)$, the force and torque caused by incident and diffracted waves. These forces are all functions of the frequency dependent hydrodynamic coefficients acquired from AQWA. Therefore, prior to running a simulation, the desired wave frequency must be specified, so that the corresponding hydrodynamic coefficients can be selected. Equations 1-2 show the expressions for $F_{rad}(t)$ and $F_B(t)$.

$$F_{rad}(t) = \begin{bmatrix} A_{11} & A_{13} & A_{15} \\ A_{31} & A_{33} & A_{35} \\ A_{51} & A_{53} & A_{55} \end{bmatrix} * \begin{Bmatrix} \ddot{x}_1 \\ \ddot{x}_3 \\ \ddot{x}_5 \end{Bmatrix} + \begin{bmatrix} C_{11} & C_{13} & C_{15} \\ C_{31} & C_{33} & C_{35} \\ C_{51} & C_{53} & C_{55} \end{bmatrix} * \begin{Bmatrix} \dot{x}_1 \\ \dot{x}_3 \\ \dot{x}_5 \end{Bmatrix} \tag{1}$$

$$F_B(t) = \begin{bmatrix} K_{11} & K_{13} & K_{15} \\ K_{31} & K_{33} & K_{35} \\ K_{51} & K_{53} & K_{55} \end{bmatrix} * \begin{Bmatrix} x_1 \\ x_3 \\ x_5 \end{Bmatrix} \tag{2}$$

The diagonal terms of the added mass, radiation damping and hydrostatic stiffness matrices are the primary hydrodynamic coefficients, i.e. how motion in that degree of freedom affects the forces in that degree of freedom. While the off diagonal terms create a coupling between the different degrees of freedom, i.e. how motion in one degrees of freedom affects the forces in another degree of freedom. Moreover, the subscripts "1, 3, and 5", refer to surge, heave, and pitch motion respectively. For more information on linear wave theory, and the hydrodynamic formulation used in this study, the WEC-Sim theory manual is a good resource (National Renewable Energy Laboratory and National Technology & Engineering Solutions of Sandia, LLC (NTESS) (2022)).

2.2 Turbine Models

A diagram of the semisubmersible platform, including the center column and three main outer columns is shown in figure 1. For this study, three separate models are developed:

(1) Baseline model containing no structural control
(2) TMD model containing a TMD in each of the three outer columns
(3) Optimal TID model containing an optimal TID in each of the three outer columns

All models are representative of the National Renewable Energy Laboratory's (NREL) 5MW reference wind turbine turbine, mounted onto a revised version of the semisubmersible platform, also developed by NREL (Jonkman et al. (2009), Robertson et al. (2014)).

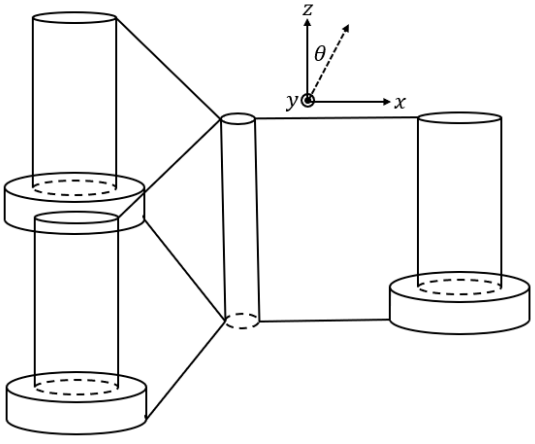

Fig. 1. Baseline platform with no structural control

Diagrams of the TMD and TIDs to be added to models 2 and 3 are shown in figure 2a and 2b, respectively. The TMD includes the standard spring and damper, while the TID also includes an inerter, and an additional spring connecting the damper and inerter to the mass via an intermediate point. The subscripts follow the same notation discussed in the following paragraphs. The baseline model is a 3 degree of freedom (DOF) model of surge (x_1), heave (z_1), and pitch (θ_1) about the turbines center of gravity (CG).

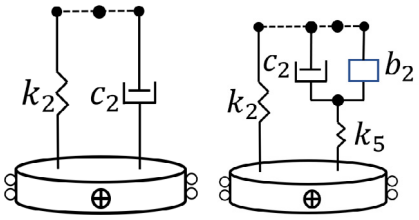

(a) Traditional TMD (b) Optimal TID

Fig. 2. Diagrams of the structural control methods implemented into the platform

The TMD model is a 6DOF model of surge, heave, and pitch about the turbines CG, as well as the relative distance between the CG of each TMD to the top of its respective column (L_2, L_3, and L_4). The masses are numbered in the following order: 1. platform, 2. mass in front left column, 3. mass in right column, and 4. mass in the back left column. So L_2 refers to the distance between the front left column and it's corresponding mass. The numbering of the stiffness, damping, and inerter values follow the same numbering notation.

The optimal TID model is a 9DOF containing the same DOFs as the TMD model, with the addition of the relative distances between the top of the columns and their respective intermediate points (L_5, L_6, and L_7). The subscript 5 refers to the distance between the top of the front left column to the corresponding intermediate point and so forth. The additional springs follow this same numbering notation.

The equations of motion are derived using the Euler-Lagrange's equation, shown in equation 3.

$$\frac{d}{dt}\frac{\partial L}{\partial \dot{q}_i} - \frac{\partial L}{\partial q_i} + \frac{\partial R}{\partial \dot{q}_i} = 0 \tag{3}$$

Where L is a quantity defined as the Lagrangian and is equal to the systems kinetic energy minus its potential energy. $\dot{q}_i$ and q_i represent the position and velocity terms for the "ith" degree of freedom. And R is defined as the Rayleigh dissipation function. Therefore, the first step to deriving the equations of motion for each model is to define their kinetic and potential energy and Rayleigh dissipation function. However, given that the baseline model is only 3DOF, it is possible to easily derive its equations of motion, shown in equation 4.

$$\begin{bmatrix} m_1 & 0 & 0 \\ 0 & m_1 & 0 \\ 0 & 0 & J_1 \end{bmatrix} * \begin{Bmatrix} x_1(t) \\ z_1(t) \\ \theta_1(t) \end{Bmatrix} = -F_{rad}(t) - F_B(t) \tag{4}$$

Where m_1 and J_1 are the mass and inertia of the platform respectively. For the TMD and optimal TID models, the equations of motion were derived symbolically using MATLAB, so for this paper, only T, U, and R are presented. For the TMD model, these quantities are defined by equations 5-7.

$$\begin{aligned} T =& \frac{1}{2}m_1\dot{x}_1^2 + \frac{1}{2}m_1\dot{z}_1^2 + \frac{1}{2}(J_1+J_2+J_3+J_4)\dot{\theta}_1^2 + \\ & \frac{1}{2}m_2\dot{x}_2^2 + \frac{1}{2}m_2\dot{z}_2^2 + \frac{1}{2}m_3\dot{x}_3^2 + \frac{1}{2}m_3\dot{z}_3^2 + \frac{1}{2}m_4\dot{x}_4^2 + \\ & \frac{1}{2}m_4\dot{z}_4^2 \end{aligned} \tag{5}$$

$$U = \frac{1}{2}k_2(L_{2,0}-L_2)^2 + \frac{1}{2}k_3(L_{3,0}-L_3)^2 + \frac{1}{2}k_4(L_{4,0}-L_4)^2 \tag{6}$$

$$R = \frac{1}{2}c_2\dot{L}_2^2 + \frac{1}{2}c_3\dot{L}_3^2 + \frac{1}{2}c_4\dot{L}_4^2 \tag{7}$$

Where $\dot{x}_2$ and $\dot{z}_2$ are the velocity in the x and z direction for the mass in the front left column, and so forth. These quantities are defined using vector geometry and are functions of the platforms pitch angle over time. $L_{2,0}$, $L_{3,0}$, and $L_{4,0}$ are the initial distance between the top of the columns and their corresponding TMD.

T, U, and R for the optimal TID model are defined by equations 8-10.

$$\begin{aligned} T =& \frac{1}{2}m_1\dot{x}_1^2 + \frac{1}{2}m_1\dot{z}_1^2 + \frac{1}{2}(J_1+J_2+J_3+J_4)\dot{\theta}_1^2 + \\ & \frac{1}{2}m_2\dot{x}_2^2 + \frac{1}{2}m_2\dot{z}_2^2 + \frac{1}{2}m_3\dot{x}_3^2 + \frac{1}{2}m_3\dot{z}_3^2 + \frac{1}{2}m_4\dot{x}_4^2 + \\ & \frac{1}{2}m_4\dot{z}_4^2 + \frac{1}{2}b_2\dot{L}_5^2 + \frac{1}{2}b_3\dot{L}_6^2 + \frac{1}{2}b_4\dot{L}_7^2 \end{aligned} \tag{8}$$

$$\begin{aligned} U =& \frac{1}{2}k_2(L_{2,0}-L_2)^2 + \frac{1}{2}k_3(L_{3,0}-L_3)^2 + \\ & \frac{1}{2}k_4(L_{4,0}-L_4)^2 + \\ & \frac{1}{2}k_5((L_{2,0}-L_{5,0})-(L_2-L_5))^2 + \\ & \frac{1}{2}k_6((L_{3,0}-L_{6,0})-(L_3-L_6))^2 + \\ & \frac{1}{2}k_7((L_{4,0}-L_{7,0})-(L_4-L_7))^2 \end{aligned} \tag{9}$$

$$R = \frac{1}{2}c_2\dot{L}_5^2 + \frac{1}{2}c_3\dot{L}_6^2 + \frac{1}{2}c_4\dot{L}_7^2 \tag{10}$$

Where $L_{5,0}$, $L_{6,0}$, and $L_{7,0}$ are the initial distance between the top of the columns and their corresponding intermediate points. For the TMD and optimal TID models, the tuned parameters of stiffness, damping, and inertance are constant between all the columns, i.e. k_2, k_3, and k_4 all share the same value. This design choice allows for a simpler optimization problem and is likely more realistic when considering real world manufacturing capabilities. As mentioned earlier, the Euler-Lagrange equation is carried out for equations 5-7 and 8-10 using MATLAB's symbolic toolbox. The resulting solution is directly formatted for

MATLAB's differential equation solvers, in order to solve for the desired motions.

Table 1. Property values used for model optimization

System Properties			
Property	**Value**	**Property**	**Value**
$m_1\ (kg)$	1.407e7	$L_{2,0}\ (m)$	13.00
$J_1\ (kg-m^2)$	1.136e10	$L_{3,0}\ (m)$	13.00
$J_{2,3,4}\ (kg-m^2)$	1.5e6	$L_{4,0}\ (m)$	13.00
$L_x\ (m)$	14.435	$L_{5,0}\ (m)$	6.50
$L_z\ (m)$	21.89	$L_{6,0}\ (m)$	6.50
		$L_{7,0}\ (m)$	6.50

The physical values used for the optimizations presented in section 3 are shown in table 1. Where L_x, and L_z are the x and z distances from the platforms CG to the center of the left columns. These quantities are used when defining the velocities of the hanging masses. The masses and inertias are taken directly from the reports discussed earlier, and the initial positions of the masses are chosen such that they are directly in the center of the main columns.

2.3 Model Validation

The method used for validating the models derived in this study is using WEC-Sim Laboratory and National Technology & Engineering Solutions of Sandia (2022). WEC-Sim is an open-source modeling tool developed by the National Renewable Energy Laboratory and Sandia National Laboratory for modeling fluid structure interactions using linear potential flow theory. Given that the models used in this study utilize the same method for modeling hydrodynamics, it makes WEC-Sim an ideal tool for validation. With that being said, WEC-Sim, does not currently have the functionality for modeling the optimal TID configuration within the platform. For this reason, only the baseline and TMD models are validated using this method. However, given that the optimal TID model is just an extension of the TMD model, with identical hydrodynamics, validation of the TMD model is considered sufficient for this study.

The validation is completed by running two nearly identical free decay tests using both WEC-Sim and the derived models. The results are plotted, and the root mean square (RMS) values of the responses are compared with each other. The free decay tests include a heave decay test with a one meter drop, and a pitch decay test with a five degree initial rotation. These results of the heave free decay tests for the TMD configuration, including the platform's heave response and position of the second tuned mass over time, are shown in figure 3.

Visually, figure 3 shows the models being nearly identical, and this is further confirmed by comparing the RMS values of the responses. For the baseline free decay tests, the RMS values were identical to three decimal places. The same can be seen, for the TMD configuration's heave free decay test, while the pitch free decay test saw only a 2% difference. This difference could be attributed to the WEC-Sim model handles pretension for a pitching system. Regardless, this 2% difference is considered acceptable for this validation.

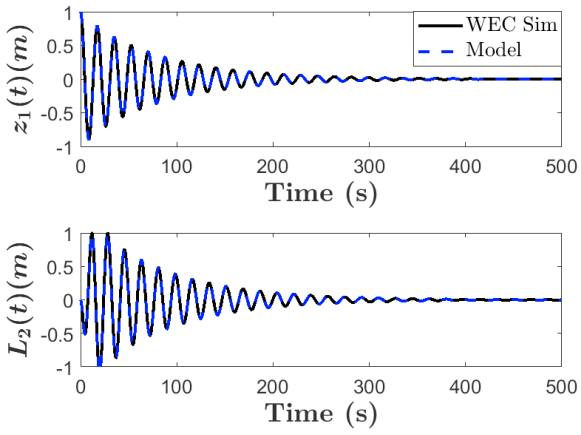

Fig. 3. Heave free decay test comparison between WEC-Sim and the derived model for the **TMD** configuration

2.4 Optimization Integration

The optimizations in this study are conducted using the "pattern search" algorithm within MATLAB's global optimization toolbox. Several different optimizations algorithms were tested for this study, however, the "pattern search" algorithm is ultimately selected based on its ability to consistently settle on the global minimum value of the objective function. In short, an optimization algorithm seeks to explore a defined design space by varying design parameters and tracking the resulting change in objective function. A surface showing this design space i.e., objective function vs. design parameters, for the TMD, heave free decay optimization is presented in figure 4.

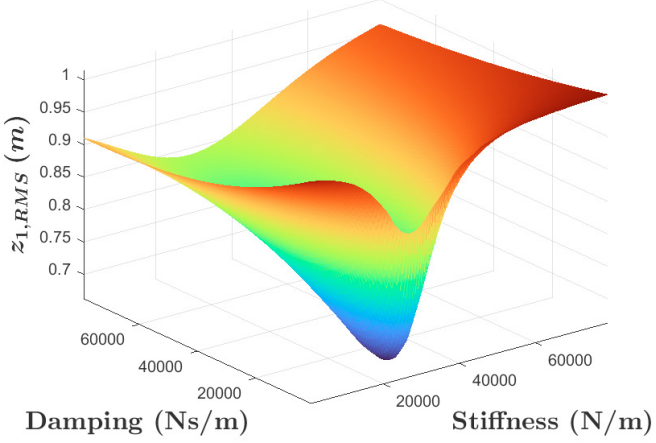

Fig. 4. Surface showing the objective function of the heave free decay optimization as a function of the design parameters

As shown on the z-axis of figure 4, the objective function for the free decay optimizations is the RMS value of the platform heave or pitch response. The design parameters are the stiffness and damping, for the TMD configuration, and the stiffness, damping, inertance, and additional stiffness, for the optimal TID configuration. The RMS values

for the objective functions are calculated using equation 11.

$$\theta_{1,RMS} = \sqrt{\frac{1}{N}\sum_{i=0}^{N}\theta_1(\Delta t * i)^2} \quad (11)$$

Where θ_1 is the systems pitch position at each time step, $\Delta t * i$. For the optimization, the simulations are run for 250 seconds with a time step of 0.01 seconds. This results in an N value equal to 25,000.

The free decay optimizations are conducted for a range of different mass ratios, μ. For this study the mass ratio is defined as the ratio of the total mass used for control over the total turbine mass. This mass ratio is used to determine $m_{2,3,4}$ for both the TMD and TID configurations. Mass ratios are commonly used for structural control related analyses as it provides a way to tie the secondary mass to the primary mass. This calculation is shown in equation 12.

$$m_{2,3,4} = \frac{\mu * m_1}{3} \quad (12)$$

The value is divided by three since there are three tuned masses in total. For each mass ratio, the free decay optimizations are conducted and the following values are recorded: optimal parameters and optimal RMS values. Using these optimal RMS values, the percent reduction from the baseline RMS value is calculated using equation 13,

$$\%\ Reduction = \frac{RMS_{Baseline} - RMS_{Control}}{RMS_{Baseline}} * 100 \quad (13)$$

where $RMS_{Baseline}$ is the RMS value calculated from the free decay response of the baseline configuration. And $RMS_{Control}$ is the RMS value calculated from the free decay response of either the TMD or optimal TID configurations. These percent reduction values are plotted at each mass ratio so that further conclusions can be drawn regarding the trends of the data. Curves are also fit to the data so that the performance of both control methods can be more accurately analyzed.

3. RESULTS

3.1 Free Decay Optimization

Figure 5 shows the optimized pitch free decay responses of the platform for a 5% mass ratio. This figure visually shows the benefit of adding structural control, since the TMD and optimal TID responses settled much faster than the baseline. Figure 5 also shows that the optimal TID configuration settles faster than the TMD configuration.

The results of the heave and pitch free decay optimizations for four different mass ratios are shown in table 2 and 3 respectively. These tables includes the RMS values for the baseline and structural control configurations, as well as the percent reduction values.

Tables 2 and 3 show that both control configurations provide a significant reduction to $RMS_{Baseline}$. With the lowest percent reduction in heave and pitch for either configuration still coming out to 18.92% and 12.27% respectively. The tables also show that increasing the mass ratio results in a significant increase in percent reduction. For example, the percent reductions at mass ratios of 1% and 7% for the heave decay test are 18.92% and 38.02%, respectively. That is nearly a +20% increase in reduction for only a +6% increase in mass ratio. Though perhaps the biggest takeaway from these results is that the optimal TID configuration outperforms the TMD configuration for both decay tests at all mass ratios. The extent to which the optimal TID outperforms the TMD varies depending on mass ratio, with the largest performance gains occurring at the larger mass ratios.

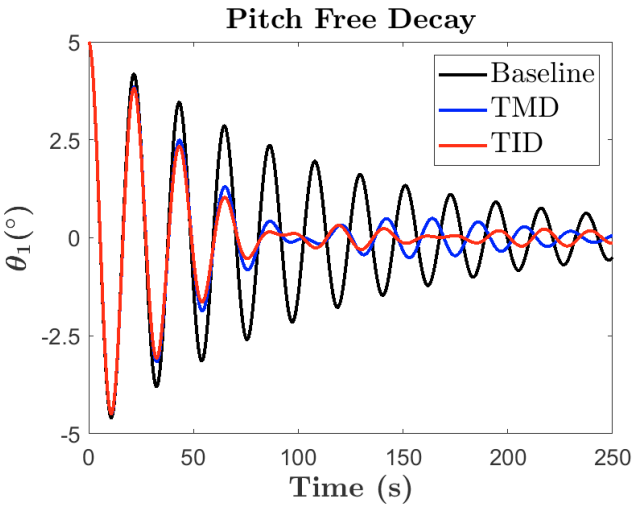

Fig. 5. Optimized pitch free decay response for the overall system with a mass ratio of 5%

Table 2. Results of the heave free decay optimizations

Heave Free Decay				
	Platform + TMD		Platform + TID	
μ	RMS (m)	% Reduction	RMS (m)	% Reduction
Baseline	1.008	-	1.008	-
0.01	0.817	18.92%	0.801	20.18%
0.03	0.713	29.29%	0.686	32.51%
0.05	0.660	34.55%	0.631	38.36%
0.07	0.625	38.02%	0.596	42.22%

Table 3. Results of the pitch free decay optimizations

Pitch Free Decay				
	Platform + TMD		Platform + TID	
μ	RMS (°)	% Reduction	RMS (°)	% Reduction
Baseline	1.804	-	1.804	-
0.01	1.582	12.27%	1.579	12.47%
0.03	1.447	19.75%	1.413	21.68%
0.05	1.366	24.27%	1.321	26.76%
0.07	1.307	27.55%	1.260	30.16%

Figure 6 shows the percent reduction as a function of mass ratio for both configurations. Curves are fit to the data points using a second-order logarithmic function.

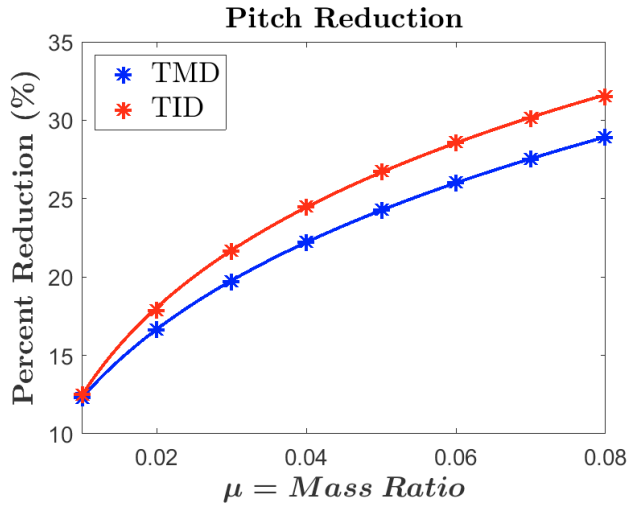

Fig. 6. Percent reduction vs. mass ratio for pitch free decay optimizations

Figure 6 further highlights the trends seen in tables 2 and 3. The optimal TID configuration outperforms the TMD configuration, and the performance gap increases as the mass ratio increases. The figure also shows that the relationship between percent reduction and the mass ratio is logarithmic, with rate of increase starting off relatively large then tapering off to a more constant value. This curve fitting analysis can also be used to determine what mass ratio for the optimal TID configuration would provide the same benefit as the TMD at a given mass ratio. For example, the optimal TIDs at a mass ratio of 5.5% would provide roughly the same benefit as the TMDs at a mass ratio of 8%. That results in roughly 250,000 kg in reductions to the physical mass needed for structural control.

4. CONCLUSION

This study has analyzed the potential benefits of implementing passive structural control systems into a semisubmersible offshore floating wind platform. Three models were derived including a baseline model with no structural control, a TMD model, and an optimal TID model. Optimizations were conducted for heave and pitch free decay tests and results were compared between the two structural control methods. Results showed that both control methods provide significant reductions compared to baseline. With the TMD configuration providing as much as 38% and 28% reduction to the heave and pitch response respectively. Furthermore, the optimal TID provided the greatest reductions for all tests conducted, outperforming the TMD by as much as 4%. The optimal TID configuration was therefore able to provide similar reduction using smaller mass ratios, allowing for a large reduction to the physical mass needed for the structural control.

ACKNOWLEDGEMENTS

The authors greatly acknowledge funding by the National Offshore Wind Research and Development Consortium (NOWRDC) and the New York State Energy Research and Development Authority (NYSERDA) (NOWRDC #123 / NYSERDA #154631).

REFERENCES

Frahm, H. (1911). Device for damping vibrations of bodies. US Patent 989,958.

Hu, Y., Wang, J., Chen, M.Z., Li, Z., and Sun, Y. (2018). Load mitigation for a barge-type floating offshore wind turbine via inerter-based passive structural control. *Engineering Structures*, 177, 198–209.

Jonkman, J., Butterfield, S., Musial, W., and Scott, G. (2009). Definition of a 5-mw reference wind turbine for offshore system development. Technical report, National Renewable Energy Lab.(NREL), Golden, CO (United States).

Laboratory, N.R.E. and National Technology & Engineering Solutions of Sandia, L.N. (2022). Wec-sim. `https://github.com/WEC-Sim/WEC-Sim`.

Lackner, M.A. and Rotea, M.A. (2011). Passive structural control of offshore wind turbines. *Wind energy*, 14(3), 373–388.

Lee, C. and Newman, J. (2013). *WAMIT User Manual*. WAMIT Inc., Chestnut Hill, MA. URL `https://www.wamit.com/manualupdate`.

Ma, R., Bi, K., and Hao, H. (2020). Heave motion mitigation of semi-submersible platform using inerter-based vibration isolation system (ivis). *Engineering structures*, 219, 110833.

Musial, W., Spitsen, P., Duffy, P., Beiter, P., Marquis, M., Hammond, R., and Shields, M. (2022). Offshore wind market report: 2022 edition. Technical report, National Renewable Energy Lab.(NREL), Golden, CO (United States).

National Renewable Energy Laboratory and National Technology & Engineering Solutions of Sandia, LLC (NTESS) (2022). Theory manual. URL `https://wec-sim.github.io/WEC-Sim/master`.

Robertson, A., Jonkman, J., Masciola, M., Song, H., Goupee, A., Coulling, A., and Luan, C. (2014). Definition of the semisubmersible floating system for phase ii of oc4. Technical report, National Renewable Energy Lab.(NREL), Golden, CO (United States).

Robertson, A.N. and Jonkman, J.M. (2011). Loads analysis of several offshore floating wind turbine concepts. In *The twenty-first international offshore and polar engineering conference*. OnePetro.

Si, Y., Karimi, H.R., and Gao, H. (2014). Modelling and optimization of a passive structural control design for a spar-type floating wind turbine. *Engineering structures*, 69, 168–182.

Smith, M.C. (2002). Synthesis of mechanical networks: the inerter. *IEEE Transactions on automatic control*, 47(10), 1648–1662.

Stewart, G.M. (2012). Load reduction of floating wind turbines using tuned mass dampers.

Zhou, B., Zhang, Z., Li, G., Yang, D., and Santos, M. (2023). Review of key technologies for offshore floating wind power generation. *Energies*, 16(2), 710.